DOI 10.1590/s1982-21702024000100005

SPECIAL SECTION - Brazilian Colloquiums on Geodetic Sciences

Contribution of SAR/Sentinel-1 images in the detection of burnt areas in the natural vegetation of the brazilian Pantanal biome

Aline Barroca Marra[1] - ORCID: 0000-0001-7311-7312

Maria de Lourdes Bueno Trindade Galo[1] - ORCID: 0000-0002-1726-3152

Edson Eyji Sano[2] - ORCID: 0000-0001-5760-556X

[1] Universidade Estadual Paulista "Júlio de Mesquita Filho" (UNESP), Cartography, Presidente Prudente – São Paulo, Brazil.
E-mail: aline.barroca@unesp.br; trindade.galo@unesp.br

[2] Embrapa Cerrados, Planaltina - Distrito Federal, Brazil.
E-mail: edson.sano@embrapa.br

Received in 31st July 2023.
Accepted in 28th November 2023.

Abstract:

The Brazilian Pantanal biome, known for its rich biodiversity and wetlands, is experiencing frequent and destructive fires. Detecting and monitoring burnt areas is vital for comprehending their present ecological condition, a key indicator for climate change and protective measures. Optical remote sensing methods, traditionally used in fire mapping, have limitations due to atmospheric conditions. Microwave Synthetic Aperture Radar (SAR) is a promising alternative, excelling in challenging environments and demonstrating sensitivity to surface properties. This study aimed to assesses the potential of SAR images for detecting burnt areas in a conservation unit inserted in the Brazilian Pantanal after intense fires in 2020. For this, the Normalized Burn Ratio (NBR) index was calculated from Sentinel-2 images before and after fire, and then the difference between these images (dNBR). Differences in backscatter coefficients of pre- and post-fire SAR/Sentinel-1 images in the two polarizations (dVH and dVV) were also calculated. To detect burnt areas, the three differences were classified using the Random Forest algorithm. The results showed adequate coincidence of burned areas between dVH and dVV compared to dNBR and high accuracy values of the algorithm model, indicating consistency between SAR and optical data in identifying burnt areas.

Keywords: Burnt area detection; Forest fire; Sentinel-1; Brazilian Pantanal; Remote sensing; Synthetic Aperture Radar.

How to cite this article: MARRA AB, GALO MLBT, SANO EE. Contribution of SAR/Sentinel-1 images in the detection of burnt areas in the natural vegetation of the brazilian Pantanal biome. *Bulletin of Geodetic Sciences*. 30: e2024005, 2024.

1. Introduction

The Pantanal biome is one of the richest and most important regions in Brazil and South America in terms of biodiversity and ecosystems. It is recognized as one of the largest wetlands in the world and covers an area of approximately 150,000 km², extending across parts of Brazil, Bolivia, and Paraguay. Most of the Pantanal is located in western Brazil, in the states of Mato Grosso and Mato Grosso do Sul (WWF, 2023).

The Pantanal is known for its rich biological diversity, harboring a wide variety of fauna and flora species. Furthermore, the biome can store water during the rainy season and gradually releasing it during the dry season. This process of hydrological regulation is essential for the maintenance of local ecosystems and for the water supply to other regions. However, the Pantanal biome has been facing one of the biggest water crises in its recent history. With scarcer rainfall, the dry season has extended throughout the year and the fire occurrence has become increasingly frequent and devastating in the biome, putting its biodiversity at risk (WWF-Brasil, 2020).

The Brazilian program Queimadas, developed by the National Institute for Space Research (Instituto Nacional de Pesquisas Espaciais, INPE) with the primary purpose of monitoring burnt areas and active fires, using remote sensing technology and satellites, estimated that 40,606 km² of the Brazilian Pantanal region was affected by fires only from January to October 2020 (INPE, 2020). More than 20% of the entire extension of the Pantanal was consumed by fires, showing an increase of approximately four times greater compared to the entire previous year (Libonati et al., 2020). The Queimadas program also shows that, of the 742,977 hotspots that occurred in the biome throughout 2020, 89% were from June 20 to November 22.

Conservation units represent the best strategy for protecting the world's natural heritage, as they safeguard the fauna and flora, as well as the processes that govern ecosystems, ensuring the maintenance of biodiversity, in addition to protecting native populations (Arruda, 1999). Federal and state conservation units inserted in the Pantanal aroused concern during the period of intense fires of 2020 as they were seriously affected. Among the conservation units, the Encontro das Águas State Park (EASP) inserted in the Pantanal of Mato-Grosso, Brazil, was one of the most affected, where a large part of its extension was consumed by fire, threatening the preservation of its flora and fauna.

In this sense, the detection and monitoring of burnt areas in the Pantanal of Mato-Grosso is of unique importance for the preservation of its biodiversity. Historically, optical remote sensing has enabled efficient detection and mapping of burnt areas (Elhag et al. 2020) and, increasingly, access fire severity through the pre- and post-fire difference of the Normalized Burn Ratio (dNBR) spectral index (Delcourt et al., 2021; Bright et al., 2019). However, the acquisition of optical data used to calculate the NBR index is subject to favorable meteorological conditions. Therefore, sensors operating in the microwave spectrum, specifically orbital Synthetic Aperture Radar (SAR) systems, become attractive in the monitoring of burnt areas, due to the minimal interference caused by clouds and smoke, allowing the acquisition of data independent of the atmospheric condition and solar radiation (Zhou et al., 2019; Tariq et al., 2021; Ban et al. 2020; Radman et al., 2023).

Different characteristics of the earth's surface features can be discriminated in SAR images. According to Jensen (2009), the information extracted from SAR images is formed mainly by sensor parameters, such as wavelength, wave polarization, spatial resolution and sensor imaging geometry, and parameters related to objects in the scene, such as topography, surface roughness, geometry of the object, object orientation and dielectric constant (directly related to soil moisture). Gibson et al. (2023), show that radar sensors are sensitive to variations in the backscattered signal, mainly caused by changes in surface roughness and soil moisture content due to the occurrence of fires. Therefore, the use of SAR images is of paramount importance for the detection and characterization of burnt areas, as it overcomes limitations imposed by adverse atmospheric conditions faced by optical data and provides detailed information on the extent and impact of forest fires.

The purpose of this study was therefore to map burnt areas in the EASP conservation unit in the dry season of 2020 based on the classification of SAR images from Sentinel-1 and compare the results with the product obtained from the classification of the pre- and post-fire difference of Sentinel-2 optical images derived from the NBR spectral index.

2. Materials and Methods

2.1 Study Area

The study was carried out at EASP, a Brazilian integral protection conservation unit under the responsibility of the Department of the Environment of the state of Mato Grosso (Secretaria de Meio Ambiente, SEMA). This region is the catchment basin for several significant rivers, including the Cuiabá, Piquiri, Pirigara, Cassange, Três Irmãos, and Alegre River (CNUC, 2023). Established in 2004 through Decree Nº. 4,881 on December 22, the park encompasses an approximate area of 108,128.69 hectares and is situated within the Pantanal biome in the southern region of the state, as illustrated in Figure 1. This Figure displays, additionally, the EASP in true-color composite of Sentinel-2 optical images obtained before (June 20, 2020) and after (November 22, 2020) a period of intense wildfires in 2020. EASP was the conservation unit most affected by fire in the state of Mato-Grosso in the dry season of 2020, devastating the equivalent of 83% of its territory until October (Libonati et al., 2020). The focus of this study was on fire events that took place between June 20 and November 22, 2020. Data sourced from the Queimadas program (INPE, 2020) revealed that the study area experienced a significant impact from fires during this time, with a total of 49,310 hotspots identified through satellite detection. These hotspots can be accessed via the program's database, available at the https://queimadas.dgi.inpe.br/queimadas/bdqueimadas portal.

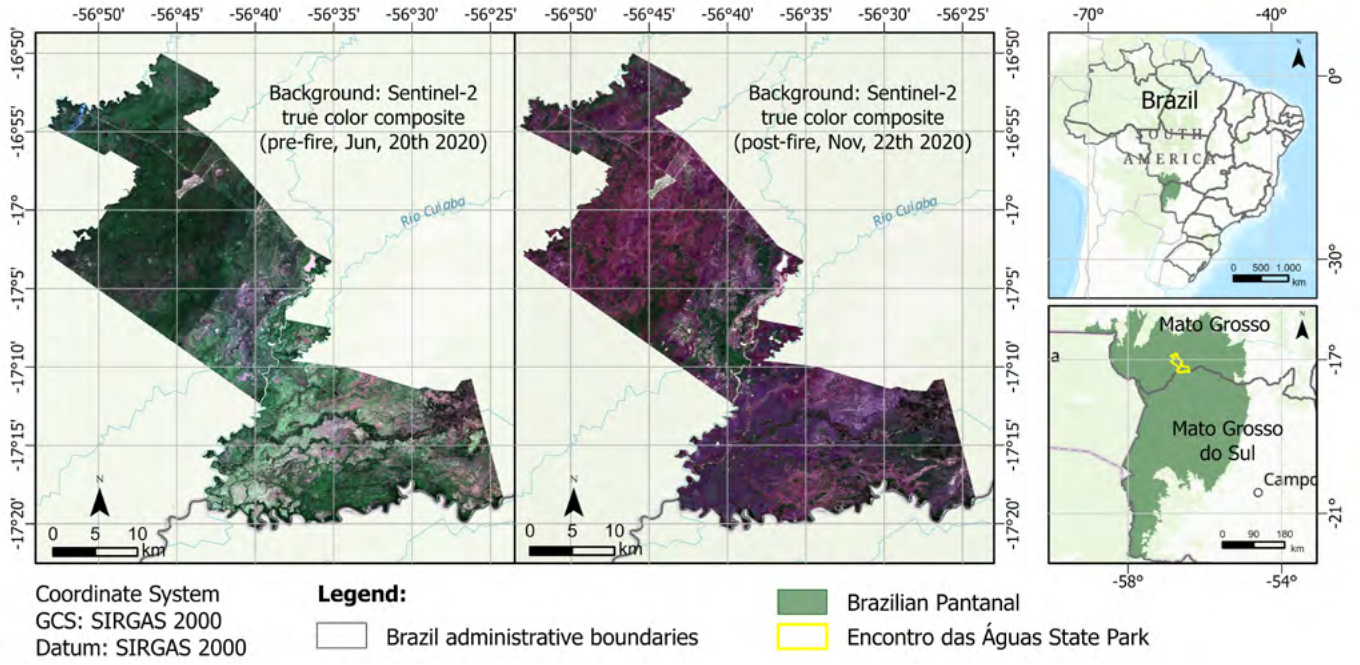

Figure 1: Location map of the study area (EASP). Left and center maps illustrate true color composite images (R4G3B2/Sentinel-2) of the park before (June 20, 2020) and after the fire (November 22, 2020), respectively.

2.2 Methodology overview

To evaluate the potential of SAR data in detecting burnt areas, some steps were followed. SAR and optical data were acquired before and after an intense period of burning in the defined study area. From the optical data, the NBR index and the dNBR from pre- and post-fire NBR images were calculated. The backscattering coefficients of the pre- and post-fire SAR images were obtained for each of the polarizations (VV and VH) and the pre- and post-fire differences were calculated, generating the difference-images in the two polarizations: dVV and dVH. The Random Forest (RF) machine learning algorithm was used to perform the individual classifications of each three differences (dNBR, dVV and dVH) in order to detect and compare the distribution of burnt areas between optical and SAR data (qualitative and quantitative comparison of classifications between dVH-dNBR and dVV-dNBR, individually). The general flowchart of the methodology can be seen in Figure 2.

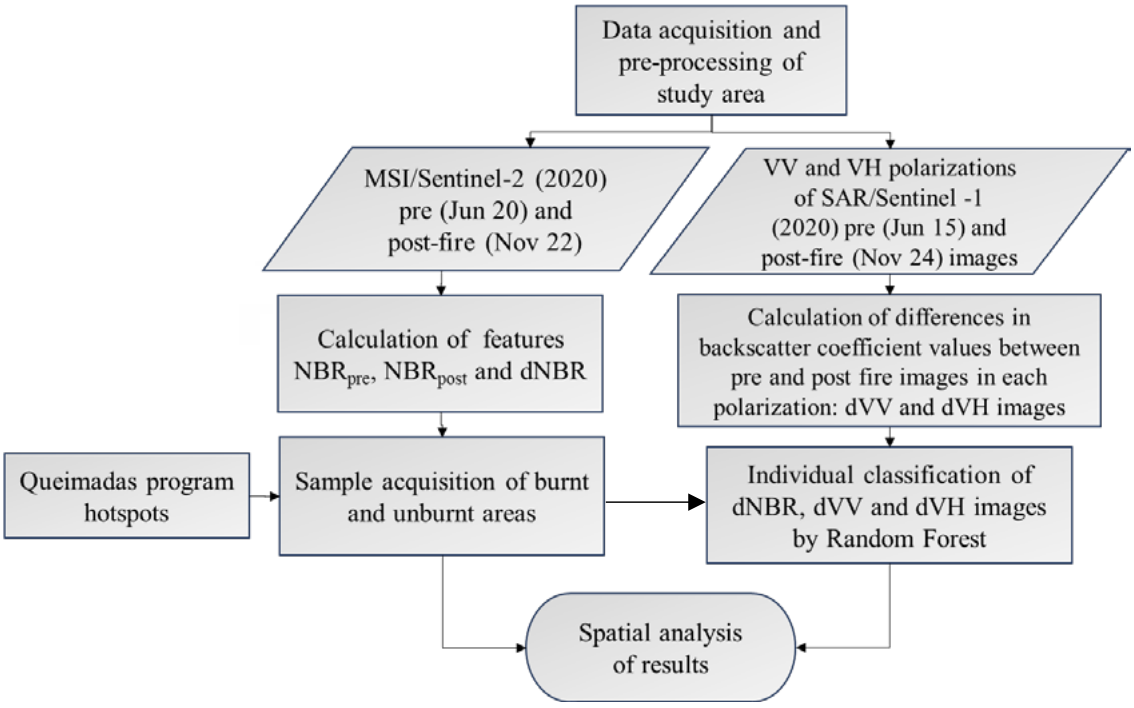

Figure 2: Overall flowchart of methodology, where NBR_{pre} and NBR_{post} refer to the Normalized Burn Ratio optical index pre- and post-fire, respectively, dNBR refers to the difference between pre- and post-fire NBRs, and dVH and dVV to the pre- and post-fire difference of SAR backscatter coefficients.

2.3 Optical and SAR data acquisition and processing

2.3.1 MSI/Sentinel-2

Copernicus Sentinel-2 is a multispectral imaging mission aiming to monitor variability in Earth's surface conditions with an orbital range of 290 km. The mission comprises a constellation of two satellites, Sentinel-2A and Sentinel-2B, in sun-synchronous polar orbit, divided 180° apart. Each Sentinel-2 satellite has revisit frequency of 10 days and the combined constellation frequency is 5 days. Sentinel-2A was launched on June 23, 2015, and Sentinel-2B on March 7, 2017, and are equipped with the MSI (MultiSpectral Instrument) sensor instrument, which provides higher spatial and spectral resolution optical images (ESA, 2023).

Sentinel-2 has 12-bit radiometric resolution and 13 spectral bands in three different spatial resolutions. The visible and near infrared (NIR) spectral bands have a spatial resolution of 10 meters, the red edge and short-wave infrared are 20 m bands and aerosol, water vapor and cirrus, 60 m. The images are available to users at different correction levels, but in this study Level-2A in atmospherically corrected Bottom Of Atmosphere (BOA) reflectance in cartographic geometry were used (ESA, 2023).

The optical images acquired on June 20 and November 22, 2020, pre- and post-fire, respectively, were resampled to 20 meters by nearest neighbor interpolation and clipped by the boundaries of the study area (EASP). All optical images were pre-processed together, however, only the spectral bands NIR (10 m) and SWIR (20 m) were effectively used.

The pre- and post-fire NBR optical index was calculated in order to discriminate burnt areas. The NBR was developed by Key and Benson (1999) and its formulation combines the use of both NIR and SWIR wavelengths (Table 1) resulting in values typically ranging from -1 to +1. Negative NBR values indicate areas that have been burned and positive values represent unburnt or less severely burnt areas. The magnitude of the negative NBR values is correlated with the severity of the burn, with more negative values indicating more extensive burn damage. This optical index, as highlighted in studies by Morante-Carballo et al. (2022) and Santos et al. (2023), is widely employed in environmental and ecological research for assessing the impact of fires on vegetation and ecosystems. It plays a crucial role in fire management and landscape monitoring by identifying the affected area's extent and facilitating post-fire recovery analysis.

Table 1: Formulations of the NBR optical spectral index and dNBR, where NIR refers to the Near-InfraRed wavelength and SWIR-1 to the Short-Wave InfraRed-1 from the Sentinel-2 sensor.

Acronym	Formulation	Reference
NBR	$\frac{\rho_{NIR} - \rho_{\mathrm{SWIR1}}}{\rho_{NIR} + \rho_{\mathrm{SWIR1}}}$	Key and Benson (1999)
dNBR	$NBR_{pre} - NBR_{post}$	Key and Benson (2006)

After calculating the NBR, the dNBR, developed by Key and Benson (2006), was calculated by taking the difference between NBR values from pre- and post-fire images (June 20 and November 22, 2020, respectively) (Table 1). The dNBR is an extension of the NBR index and provides additional information to better characterize the size and severity of the burn, particularly in the context of wildfire monitoring and post-fire analysis. Therefore, the dNBR was used as ground truth for collecting samples to be applied in the classification.

Key and Benson (2006) used dNBR to characterize fire severity, based on TM and ETM+/Landsat images, and found that higher positive dNBR values indicate areas of higher burn severity, while lower or negative dNBR values suggest less severe or unburnt areas. Therefore, the histogram of the distribution of the digital numbers of the dNBR pixels was calculated. The histogram shows the statistical frequency of pixel values distribution in image, allowing to verify the extension of pixels attributed to different levels of fire severity.

2.3.2 SAR/Sentinel-1

SAR images are the result of the backscattering process of an electromagnetic wave transmitted with a vertical (V) or horizontal (H) polarization. SAR systems can operate in both co-polarization and cross-polarization modes. The co-polarization mode occurs when the sensor antenna transmits and receives energy in the same polarization, i.e., the antenna transmits energy horizontally and receives horizontally (HH) or transmits and receives vertically (VV). In cross polarization mode, the antenna transmits and receives in different polarizations (VH or HV). The backscatter

coefficient, also known as sigma nought (σ°), is an essential parameter determined by the value of backscatter in relation to the amount of energy emitted by the microwave sensor. The power received by the radar antenna is influenced by the characteristics of the radar system, such as wavelength, wave polarization, spatial resolution, and sensor imaging geometry, as well as the characteristics of the object being imaged, such as electrical components (dielectric constant/ water content), roughness and geometry (Lillesand et al., 2015).

Surface roughness is an important characteristic of backscattered signal intensity and is directly related to the sensor wavelength. Small fluctuations in the roughness of the surface imaged by the radar affect the signal in bands with short wavelengths (X band, from 7.9 to 12.5 GHz, for example) more than in bands with longer wavelengths (L band, from 1.0 to 2.0 GHz, for example). The dielectric constant of the materials present on the surface also significantly influences the backscattering of the radar signal. The dielectric constant measures the ability of different materials (vegetation, soil, rock, water, ice, etc.) to conduct electrical energy. The dielectric constant has direct proportionality in relation to the amount of moisture in the soil. Thus, the greater the dielectric constant of the material, the greater the interaction of the electric field of the incident energy with the water and the stronger the signal return (Jensen, 2009).

The Sentinel-1 mission comprises a constellation of two satellites, Sentinel-1A and Sentinel-1B, launched on April 3, 2014, and April 25, 2016, consecutively, however, only Sentinel-1A is currently in operation. The satellites have a near-polar, sun-synchronous orbit with a 12-day repeating cycle. Sentinel-1 satellites incorporate a SAR instrument that operates in the C band at a frequency of 5.404 GHz. Interferometric Wide Swath Mode (IW) is the main mode for acquiring data on the Earth's surface with VV+VH polarization. IW mode acquires images in three sub-swaths using the Terrain Observation with Progressive Scans SAR (TOPSAR) imaging technique, avoiding clipping, and resulting in homogeneous image quality across the entire range. Data are acquired over a 250 km swath with a spatial resolution of 5 m by 20 m. SAR images can be provided in "complex" format, known as Single Look Complex (SLC), and Ground Range Detected (GRD), which consists of detected, multi-looked, and ellipsoid projected SAR data (ESA, 2023).

One of the main advantages of SAR imaging is the ability to operate independently of solar radiation, and low interference from clouds, smoke, and fog, among other meteorological conditions. This is especially important in wildfire scenarios, where the presence of clouds and smoke can obscure images from optical sensors, making it difficult to detect and assess affected areas (Lillesand et al., 2015). SAR images also offer valuable insights into the vegetation structure of burnt areas, enabling the identification of distinct patterns associated with recently affected regions. These patterns arise from changes in texture, roughness, and soil water content following a fire event. As a result, SAR analysis allows for an accurate assessment of the fire's impact on the local ecosystem. Zhou et al. (2019) show that, the backscattering process in vegetation before a fire, is mainly dominated by the volume scattering from the vegetation's canopy layer. However, following a fire, when part of the ground becomes exposed due to the burning of vegetation, the dominant mechanism shifts to surface scattering. This surface scattering is predominantly influenced by the roughness and moisture content of the soil.

In this sense, the use of SAR images has proven to be a valuable tool in detecting and monitoring burnt areas. The studies conducted by Mastro et al. (2022) and Tariq et al. (2021) affirm that C-band backscatter coefficients are highly effective in detecting fire disturbances. This efficiency stems from their sensitivity to changes in the vegetation structure, which is affected by the fire impact. SAR images is also significantly impacted by variations in soil and vegetation moisture. This influence is particularly pronounced in areas that have experienced severe burning, where the ground surface is exposed (Gibson et al., 2023).

For this study, images taken before and after the burning period, June 15, and November 24, 2020, respectively, were selected. The images were acquired from the Sentinel-1A satellite (C band), in SLC format and IW mode. To obtain the sigma nought backscatter coefficients in the VV and VH polarizations ($\boldsymbol{\sigma^0_{VV}}$ e $\boldsymbol{\sigma^0_{VH}}$) the following pre-processing were carried out: image split, defining only one sub-swath (IW2) and 4 bursts (5 to 8); orbit correction; removal of thermal noise; data calibration; deburst; multilooking with 4x1 looks (distance x azimuth); application

of the Refined Lee filter with a 3 x 3 window; and finally, terrain correction was performed based on the data from the Shuttle Radar Topography Mission (SRTM), where the image pixels were also resampled to 20m, to grant consistency with Sentinel-2 data (Figure 3). The data pre-processing, both optical and SAR images, was performed using the Sentinel Application Platform 8.0 (SNAP) software, developed by the ESA (European Space Agency).

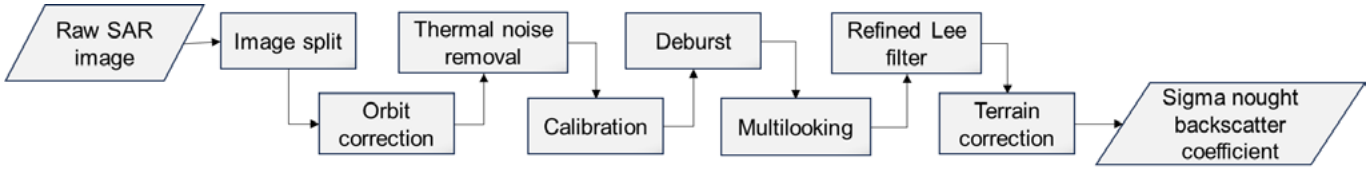

Figure 3: SAR/Sentinel-1 pre-processing workflow.

After pre-processing the SAR images, the pre- and post-fire backscatter coefficients in both polarizations ($\boldsymbol{\sigma^0_{VV}}$ e $\boldsymbol{\sigma^0_{VH}}$) were subtracted, expressed by dVV and dVH (Table 2). The pre- and post-fire differences of both backscatter coefficients of the SAR images were also calculated in order to highlight burnt surfaces in the study area and compare qualitatively and quantitatively with the result obtained through the dNBR optical measurement.

Table 2: Formulations of the SAR data differences used in this study, where $\boldsymbol{\sigma^0_{VV}}$ and $\boldsymbol{\sigma^0_{VH}}$ refer to the VV and VH backscatter coefficients from the Sentinel-1 sensor and the $_{pre}$ and $_{post}$ indices to the images taken before and after the burning period, respectively.

Acronym	Formulation
dVV	$\sigma^0_{VV,pre} - \sigma^0_{VV,\mathrm{post}}$
dVH	$\sigma^0_{VH,pre} - \sigma^0_{VH,post}$

2.4 Classification of MSI/Sentinel-2 and SAR/Sentinel-1 data

The classification of remote sensing data is a fundamental technique to detect and monitor burnt areas, contributing to the understanding of the extent, intensity and environmental impacts caused by the fire event. The RF machine learning algorithm, developed by Breiman (2001), has emerged as a powerful tool that combines multiple decision trees, introduces randomness in feature selection and data sampling, reducing overfitting and providing more robust predictions. It is widely used in machine learning applications due to its effectiveness and ability to deal with a variety of problems. This algorithm plays a significant role in the application of studies aimed at accessing the degradation of areas affected by fire due to the construction of a robust and precise predictive model, ability to deal with heterogeneous and unbalanced data, in addition to providing a measure of importance for each feature presented to the network (Jarocińska et al., 2023). Authors such as Gibson et al. (2020), Pacheco et al. (2021), and Li et al. (2023), highlight the importance of RF as an efficient and accurate algorithm for detection, mapping, and monitoring applications of burned areas.

For this study, three classifications were performed using the RF algorithm with the aim of detecting burned areas in the study area. The input data for the classification were, separately, the difference images dNBR, dVV and dVH, considering two output classes: burnt areas and unburnt areas. The dNBR was considered the ground truth for the sample collection of the two classes used in the training of the RF algorithm. Furthermore, the sample collection was performed based on the visual interpretation of the optical images in true color composite (R4G3B2/

Sentinel-2), before and after the fire (June 20 and November 22, 2020, respectively), subsidized by information on fire outbreaks acquired from the Queimadas program (https://queimadas.dgi.inpe.br/queimadas/bdqueimadas).

The samples were divided so that 70% of the pixels were used in algorithm training and 30% in model validation. To evaluate the ability of each difference image (dNBR, dVV and dVH) in detecting burned areas by the respective RF models, the Recall, Precision, F1-Score, and accuracy metrics were calculated from the validation data. In addition, the results of the classifications of the SAR dVV and dVH products were compared individually with the classified dNBR image, allowing to obtain the proportions of coincidences and disagreements between the classifications.

3. Results and discussions

3.1 Optical and SAR pre- and post-fire differences

The dNBR, calculated from the pre- and post-fire (June 20th and November 22nd, respectively) difference of the NBR optical spectral index, is shown in Figure 4. Figure 4 also shows the frequency histogram of the dNBR pixels and the NBRs generated for its calculation. Regarding the SAR data, Figure 5 shows the dVH and dVV differences (Figure 5 a and b, respectively), their respective histograms, and pre- and post-fire backscatter coefficients (June 15 and November 24, 2020, respectively).

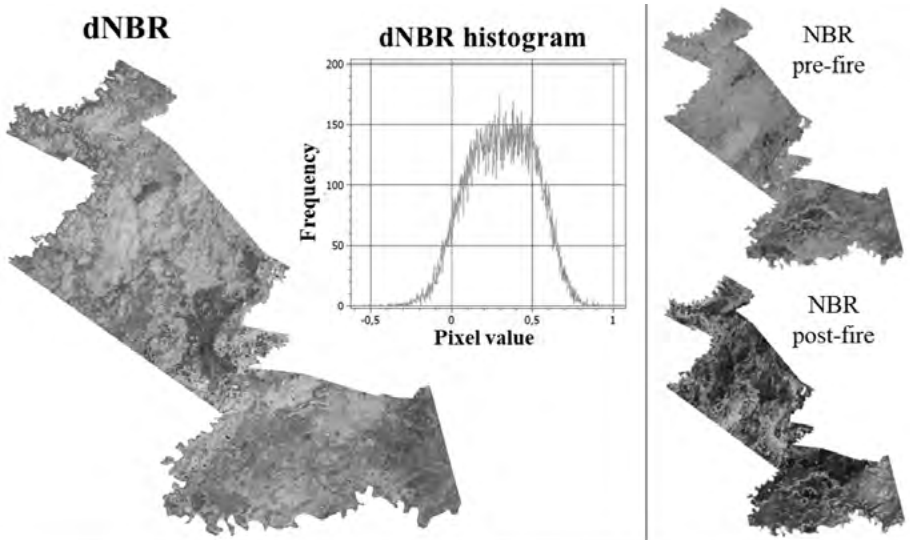

Figure 4: dNBR image used as ground truth, where areas in lighter shades of gray represent the highest degrees of burn severity and its frequency histogram. The pre- and post-fire NBRs (June 20 and November 22, 2020, respectively), used to calculate the dNBR, are shown on the right.

Since burnt areas in the NBR spectral index result in darker shades of gray after the occurrence of fire in relation to pre-fire NBR, it is understood that the areas that suffered from the action of fire respond in a lighter tone in dNBR, enhancing the detection of burnt areas, as can be seen in Figure 4. The histogram calculated for dNBR in this study shows a large variance, mainly at values above 0.1. In addition, there was a predominance of lighter gray values, above 0.1. A similar behavior, with lighter gray levels indicating burned areas, can be observed for the SAR dVV and dVH differences, in which the burnt areas also show lighter shades of gray (Figure 5 a and b).

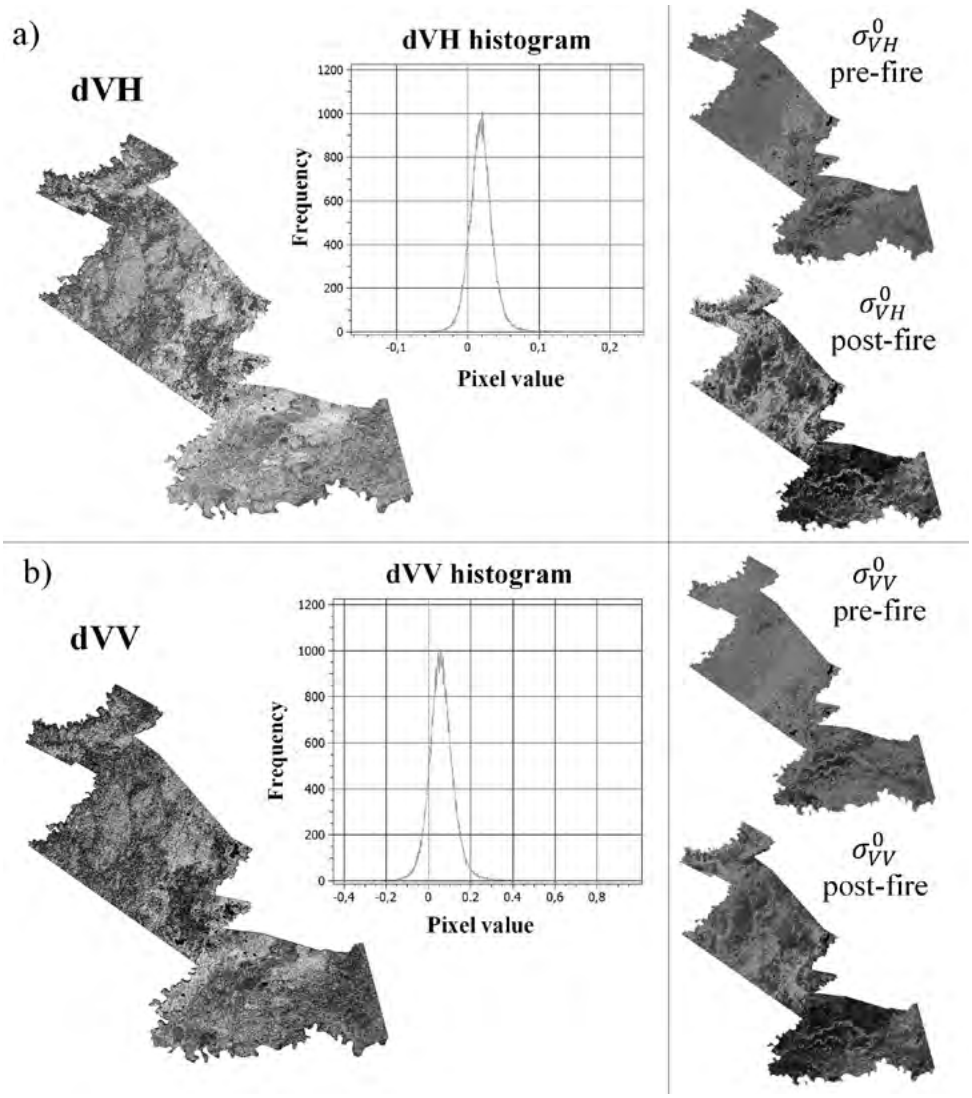

Figure 5: Difference between the backscatter coefficients of the SAR/Sentinel-1 images dVH in a) and dVV in b), accompanied by their respective frequency histograms. The pre- and post-fire backscatter coefficients (June 15 and November 24, 2020, respectively) are shown on the right side, used to calculate both differences.

All generated histograms (Figures 4 and 5), present maximum values slightly displaced from zero, each one at a different magnitude. The dNBR presented a greater number of gray level values close to the maximum frequency value of the histogram, unlike the histograms generated from the SAR differences, with a frequency peak concentrated in a few gray level values. This indicates that the burnt areas present in the SAR dVV and dVH differences are presented in a smaller variation of gray levels in relation to the dNBR optical product. From the dNBR (Figure 4), it was also observed the presence of water bodies with values around 0.4, close to the peak of the gray level values of the image pixels, which are associated with burnt areas. On the other hand, the dVH and dVV products had greater sensitivity in relation to water bodies, representing them with low brightness. This occurs due to the specular reflection of radar pulses generally suffered by bodies of water, which causes these areas to present dark levels of gray in the image (Jensen, 2009).

3.2 Burnt area classifications based on optical and SAR differences images

The spatial distribution of burnt and unburnt areas based on the dNBR, dVH and dVV classifications are shown in Figure 6 a, b, and c, respectively, where areas in red represent burnt areas and in green, unburnt areas.

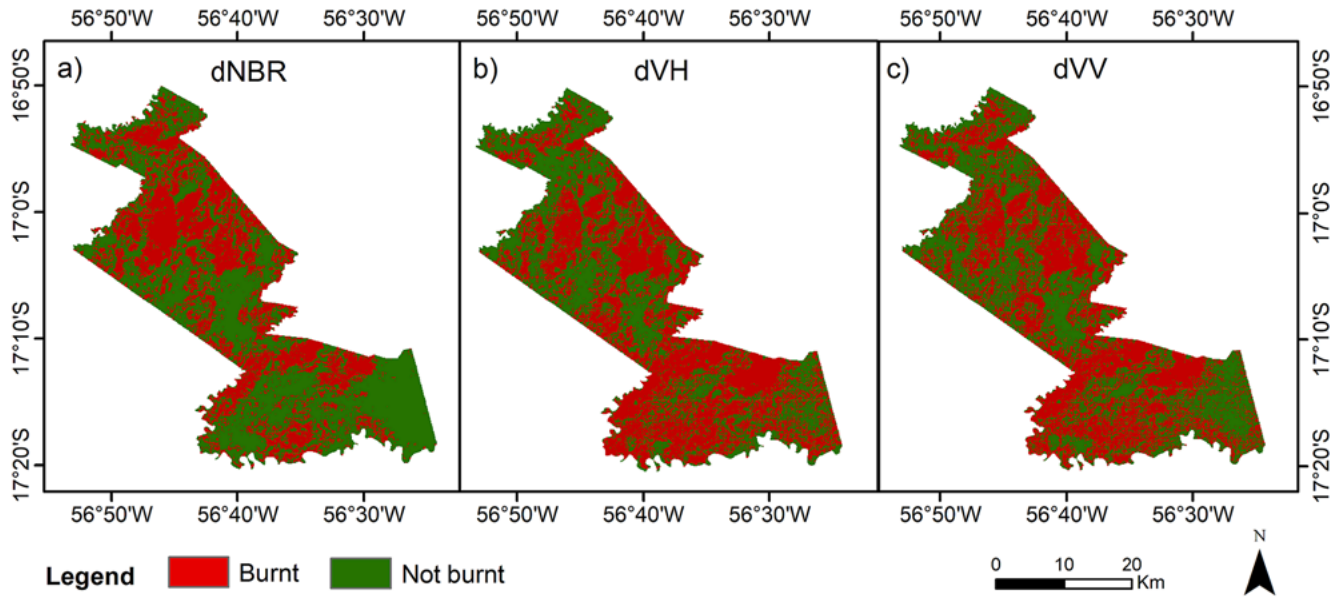

Figure 6: Classification of the differences a) dNBR, b) dVH and c) dVV, where areas in red represent burnt areas and in green, unburnt areas.

Based on the findings from the data classification, the dNBR indicated 42% of the total area as burnt, whereas the dVH and dVV SAR differences showed a larger proportion classified as burnt, 55% and 52%, respectively (Figure 6). The collection of samples used in the classifications from burnt areas was directed to the lighter gray tones that indicate greater severity of burns. Therefore, the SAR dVH and dVV differences may have detected more burnt areas in relation to the dNBR, due to the defining characteristics of the backscatter of the radar signal, such as water content and surface roughness, which might be more sensitive to lower levels of burn severity compared to optical images.

Regarding the classification's performance, Table 3 shows the Recall, Precision, F1-Score, and Accuracy metrics, resulting from the application of RF models in dNBR, dVH and dVV models on the 30% of the validation data.

Table 3: Performance of RF models in detecting burnt areas in dNBR, dVH and dVV images, expressed by Recall, Precision, F1-Score and Accuracy metrics.

	dNBR	**dVH**	**dVV**
Kappa	1.000	0.920	0.880
GA	1.000	0.960	0.940
Recall	1.000	0.972	0.942
Precision	0.998	0.946	0.928
F1-Score	0.999	0.959	0.935
Accuracy	0.999	0.962	0.940

The results estimated from the 30% of validation data indicated in Table 3 show that dNBR reached maximum values for Kappa coefficient, GA, and Recall (1.000) and presented values above 0.99 for the other metrics. All metrics calculated for dVH indicated subtly better results in relation to the dVV difference, with a 0.04 difference comparing the Kappa coefficient and 0.03 the Recall. The remaining metrics showed differences around 0.02. The maximum difference between dNBR and dVH results, which achieved the best performance among SAR data, was 0.08 for the kappa coefficient. These results indicate the consistency in the detection of burned areas by the SAR data, since the generated SAR models were able to efficiently learn and generalize the information of the samples collected from optical data.

3.3 Optical and SAR classifications comparison

Furthermore, the classifications generated for the dVH and dVV SAR differences were individually compared with the classification of the dNBR optical difference, with the objective of analyzing the coincidence of burnt areas of the SAR differences in relation to the optical difference. The results are shown in Figure 7.

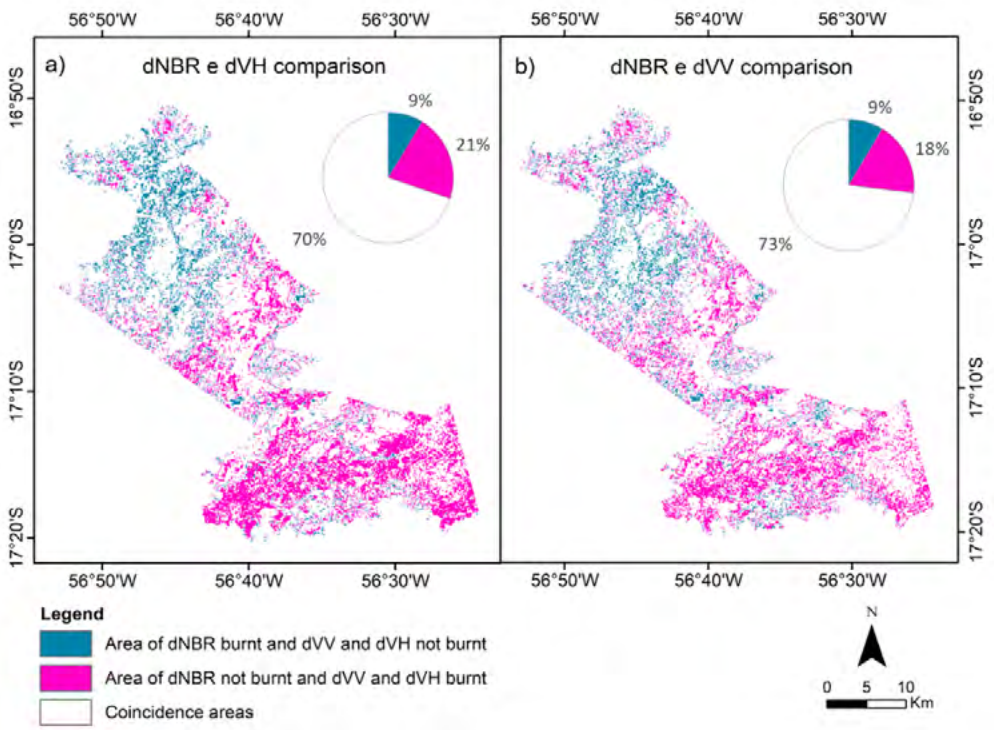

Figure 7: Thematic maps resulting from the individual comparison between the classification of a) dNBR with dVH and b) dNBR with dVV. The blue color represents unburnt areas in dVH and dVV and burnt in dNBR, the magenta color, areas burnt in dVH and dVV and unburnt in dNBR, and the white, coincident areas.

Comparing the dVH and dVV classifications individually with the dNBR classification, the results showed similar percentages of area coincidence (white areas), being 70% between dVH and dNBR (Figure 7 a), and 73% between dVV and dNBR (Figure 7 b). The results also showed that the dVH and dVV products identified more burnt areas compared to dNBR, 21% and 18%, respectively, illustrated in magenta. The areas classified as unburnt in the SAR differences and burned in the dNBR difference were only 9%, in both cases.

The obtained results indicate that SAR data, especially differences between pre- and post-fire backscatter coefficients that allow highlighting burnt areas, are sensitive to different levels of fire severity, even the samples used in the classification having been collected generally from more prominent areas in the dNBR. Gibson et al. (2023) states that the ability of C-band SAR to detect burnt areas and assess fire severity relies on its sensitivity to structural changes since the direct influence of removing leaves and twigs in the canopy was observed in the C-band backscattering response.

4. Conclusions

Forest fires pose a serious threat, especially to the Brazilian Pantanal biome which plays an essential role in providing vital ecosystem services for Brazil and the world, harboring a unique biological diversity, and regulating hydrological and climate cycles. The occurrence of fire, mainly in protected areas, constitutes one of the most important sources of alteration and destruction of flora and fauna. Monitoring fires on natural vegetation in the Pantanal biome, is of unique importance for the preservation of the biome's biodiversity. Ensuring the preservation of the Pantanal biome and its diverse functions requires the adoption of efficient fire management strategies and remote sensing techniques have already proven to be efficient in providing information about the extent and effects caused by fires.

The results of this study showed that the dVH and dVV SAR products overestimated the burnt areas in relation to the dNBR optical image, however, the SAR data indicated consistency in relation to the optical data, showing a high coincidence of areas classified as burnt and distribution spatially coincident. In addition, it is important to highlight that the dVH and dVV products were able to differentiate water bodies, not associating them with burnt areas, as occurred with dNBR.

Due to the interference of several factors related to the targets on the ground and the sensor system in the radar response, such as the wavelength in which the sensor operates and surface roughness; wave polarization; spatial resolution; target dielectric constant; among others, the interpretation of SAR data becomes quite complex and not very intuitive. However, the possibility of acquiring data in near real time allows the monitoring and accurate detection of active fire and its spread when complemented by optical data in adverse atmospheric conditions. The integration of these data with other sources of information is essential to support monitoring actions and decision-making related to the management and conservation of ecosystems affected by fire.

Finally, some additional studies are suggested, such as the evaluation of other polarimetric features and algorithms based on deep learning for the detection of burnt areas. Additionally, the analysis of time series of SAR data, together with optical features, constitutes a promising approach for monitoring the regeneration of burnt areas.

ACKNOWLEDGEMENT

The authors kindly thank the Graduate Program in Cartographic Sciences of São Paulo State University - PPGCC/Unesp. This study was supported in part by the Higher Education Personnel Improvement (CAPES – Finance Code 001, Grant Number 88887.817766/2023-00); Agricultural and Forestry Studies Foundation (FEPAF – Process Number 052) and São Paulo Research Foundation (FAPESP – Process Number 2012/06029-7).

AUTHOR´S CONTRIBUTION

Conceptualization: A.B.M. and M.L.B.T.G.; methodology: A.B.M. and M.L.B.T.G.; formal analysis: A.B.M., M.L.B.T.G. and E.E.S.; investigation: A.B.M., M.L.B.T.G. and E.E.S.; writing - Original draft preparation: A.B.M.; writing - Review and editing: A.B.M., M.L.B.T.G. and E.E.S.; visualization: A.B.M., M.L.B.T.G. and E.E.S.; supervision: M.L.B.T.G. and E.E.S.; funding acquisition: M.L.B.T.G. All authors have read and agreed to the published version of the manuscript.

REFERENCES

Arruda, R. 1999. "Populações tradicionais" e a proteção dos recursos naturais em unidades de conservação. Ambiente e Sociedade, 5, 79-92. doi.org/10.1590/S1414-753X1999000200007.

Ban, Y.; Zhang, P.; Nascetti, A.; Bevington, A. R., Wulder, M. A. 2020. Near Real-Time Wildfire Progression Monitoring with Sentinel-1 SAR Time Series and Deep Learning. Scientific Reports, 10, 1322. doi.org/10.1038/s41598-019-56967-x.

Breiman, L. 2001. Random Forests. Machine Learning, 45, 5–32. doi.org/10.1023/A:1010933404324.

Bright, B. C.; Hudak, A. T.; Kennedy, R. E; Braaten, J. D.; Khalyani, A. H. 2019. Examining post-fire vegetation recovery with Landsat time series analysis in three western North American forest types. Fire Ecology, 15, 8. doi.org/10.1186/s42408-018-0021-9.

CNUC. Cadastro Nacional de Unidades de Conservação. https://antigo.mma.gov.br/areas-protegidas/cadastro-nacional-de-ucs. Accessed 20 June 2023.

Delcourt, C. J. F.; Combee, A.; Izbicki, B.; Mack, M. C.; Maximov, T.; Petrov, R.; Rogers, B. M.; Scholten, R. C.; Shestakova, T.A.; Van Wees, D.; Veraverbeke, S. 2021. Evaluating the Differenced Normalized Burn Ratio for Assessing Fire Severity Using Sentinel-2 Imagery in Northeast Siberian Larch Forests. Remote Sensing, 13, 2311. doi.org/10.3390/rs13122311.

Elhag, M.; Yimaz, N.; Bahrawi, J.; Boteva, S. 2020. Evaluation of Optical Remote Sensing Data in Burned Areas Mapping of Thasos Island, Greece. Earth Syst Environ, 4, 813–826. doi.org/10.1007/s41748-020-00195-1.

ESA (European Space Agency). Sentinel Online. https://sentinels.copernicus.eu/web/sentinel. Accessed 15 July 2023.

Gibson, R.K.; Mitchell, A.; Chang, H.-C. 2023. Image Texture Analysis Enhances Classification of Fire Extent and Severity Using Sentinel 1 and 2 Satellite Imagery. Remote Sensing, 15, 3512. doi.org/10.3390/rs15143512.

Gibson, R.; Danaher, T.; Hehir, W., Collins, L. 2020. A remote sensing approach to mapping fire severity in south-eastern Australia using sentinel 2 and random forest. Remote Sensing of Environment, 240(111702), 0034-4257. doi.org/10.1016/j.rse.2020.111702.

INPE. 2020. Portal do Monitoramento de Queimadas e Incêndios Florestais. https://queimadas.dgi.inpe.br/queimadas/bdqueimadas. Accessed 20 June 2023.

Jarocińska, A.; Marcinkowska-Ochtyra, A.; Ochtyra, A. 2023. An Overview of the Special Issue "Remote Sensing Applications in Vegetation Classification". Remote Sensing, 15, 2278. doi.org/10.3390/rs15092278.

Jensen, J. R. 2009. Remote Sensing of the Environment: An Earth Resource Perspective, 2nd Edition. New Delhi: Pearson Education India.

Key, C. H.; Benson, N. C. 2006. Landscape assessment: Sampling and analysis methods. Firemon: Fire effects monitoring and inventory system. General Technical Report. USDA Forest Service, Rocky Mountain Research Station, Fort Collins CO., RMRS-GTR-164-CD.

Key, C. H.; Benson, N. C. 1999. The Normalized Burn Ratio (NBR): A Landsat TM radiometric measure of burn severity. U.S. Department of the Interior, Northern Rocky Mountain Science Centre.

Li, X.; Zhang, G.; Tan, S.; Yang, Z.; Wu, X. 2023. Forest Fire Smoke Detection Research Based on the Random Forest Algorithm and Sub-Pixel Mapping Method. Forests, 14, 485. doi.org/10.3390/f14030485.

Libonati, R.; Belém, L.; Rodrigues, J.; Lemos, F.; Sena, C.; Pinto, M.; Carvalho, I. A. 2020. Nota técnica LASA - Área queimada Pantanal: situação até 18 de outubro 2020. Sistema ALARMES (Alerta de Área queimada com Monitoramento Estimado por Satélite). p. 12, Rio de Janeiro, Laboratório de Aplicações de Satélites Ambientais – UFRJ. doi.org/10.13140/RG.2.2.26367.02721.

Lillesand, T.M.; Kiefer, R.W.; Chipman, J.W. 2015. Remote Sensing and Image Interpretation. Hoboken: John Wiley & Sons Inc., 7th ed.

Mastro, P.; Masiello, G.; Serio, C.; Pepe, A. 2022. Change Detection Techniques with Synthetic Aperture Radar Images: Experiments with Random Forests and Sentinel-1 Observations. Remote Sensing, 14, 3323. doi.org/10.3390/rs14143323.

Morante-Carballo, F.; Bravo-Montero, L.; Carrión-Mero, P.; Velastegui-Montoya, A.; Berrezueta, E. 2022. Forest Fire Assessment Using Remote Sensing to Support the Development of an Action Plan Proposal in Ecuador. Remote Sensing, 14, 1783. doi.org/10.3390/rs14081783.

Pacheco, A. P.; Junior, J. A. S.; Ruiz-Armenteros, A. M.; Henriques, R. F. F. 2021. Assessment of k-Nearest Neighbor and Random Forest Classifiers for Mapping Forest Fire Areas in Central Portugal Using Landsat-8, Sentinel-2, and Terra Imagery. Remote Sensing, 13(7), 1345. doi.org/10.3390/rs13071345.

Radman, A.; Shah-Hosseini, R.; Homayouni, S. 2023. A deep convolutional neural network for burn progression mapping using Sentinel-1 SAR time-series. International Journal of Remote Sensing, 44(7), 2196–2215. doi.org/10.1080/01431161.2023.2197131.

Santos, S. M. B.; Duverger, S. G.; Bento-Gonçalves, A.; Franca-Rocha, W.; Vieira, A.; Teixeira, G. 2023. Remote Sensing Applications for Mapping Large Wildfires Based on Machine Learning and Time Series in Northwestern Portugal. Fire, 6(2), 43. doi.org/10.3390/fire6020043.

Tariq, A.; Shu, H.; Li, Q.; Altan, O.; Khan, M. R.; Baqa, M. F.; Lu, L. 2021. Quantitative Analysis of Forest Fires in Southeastern Australia Using SAR Data. Remote Sensing, 13, 2386. doi.org/10.3390/rs13122386.

Zhou, Z.; Liu, L.; Jiang, L.; Feng, W.; Samsonov, S.V. 2019. Using Long-Term SAR Backscatter Data to Monitor Post-Fire Vegetation Recovery in Tundra Environment. Remote Sensing, 11, 2230. doi.org/10.3390/rs11192230.

WWF (World Wildlife Fund). 2023. 5 interesting facts about the Pantanal, the world's largest tropical wetland. https://www.worldwildlife.org/stories/5-interesting-facts-about-the-pantanal-the-world-s-largest-tropical-wetland. Accessed 10 July 2023.

WWF-Brasil (World Wildlife Fund - Brasil). 2020. Retrospectiva 2020: Pantanal teve recordes históricos de queimada. https://www.wwf.org.br/?77589/Retrospectiva-2020-Pantanal-teve-recordes-historicos-de-queimadas>. Accessed 10 July 2023.